# Hydrogen diffusion in bulk and nanocrystalline palladium: A quasielastic neutron scattering study

Maiko Kofu, Naoki Hashimoto, Hiroshi Akiba, Hirokazu Kobayashi, Hiroshi Kitagawa, Madhusudan Tyagi, Antonio Faraone, John R. D. Copley, Wiebke Lohstroh, and Osamu Yamamuro

Phys. Rev. B **94**, 064303 — Published 29 August 2016

DOI: 10.1103/PhysRevB.94.064303

# Hydrogen diffusion in bulk and nanocrystalline palladium: A quasielastic neutron scattering study

Maiko Kofu,[1] Naoki Hashimoto,[1] Hiroshi Akiba,[1] Hirokazu Kobayashi,[2] Hiroshi Kitagawa,[2] Madhusudan Tyagi,[3,4] Antonio Faraone,[3,4] John R. D. Copley,[3] Wiebke Lohstroh,[5] and Osamu Yamamuro[1,*]

[1] *Institute for Solid State Physics, University of Tokyo, Kashiwa, Chiba 277-8581, Japan*
[2] *Graduate School of Science, Kyoto University, Sakyo-ku, Kyoto 606-8502, Japan*
[3] *NIST Center for Neutron Research, National Institute of Standards and Technology, Gaithersburg, Maryland 20899-6102, USA*
[4] *Department of Materials Science, University of Maryland, College Park, Maryland 20742, USA*
[5] *Heinz Maier-Leibnitz Zentrum (MLZ), Technische Universität München, Garching D-85747, Germany*

(Dated: August 12, 2016)

The diffusion dynamics of hydrogen in bulk and nanocrystalline palladium has been examined using quasielastic neutron scattering (QENS). With respect to bulk $PdH_{0.73}$, two relaxation processes were found. For both processes, the variation of the relaxation times with momentum transfer was well reproduced by a model of jump diffusion between adjacent octahedral sites. Upon cooling the fast relaxation fraction decreases. The result suggests that the slow relaxation corresponds to jumps between the ground states and the fast one between excited states. In nanocrystalline $PdH_{0.47}$ with a size of 8 nm, we found a new fast diffusion process with a smaller activation energy in addition to the one observed in the bulk sample. The new process could be due to the motion of hydrogen atoms in the subsurface region where the potential energy surface is substantially modified by surface strain/distortion effects. This is the first QENS experiment that probes hydrogen diffusion within Pd nanoparticles.

## I. INTRODUCTION

Palladium hydride ($PdH_x$) is a prototypical metal hydride which has been studied extensively in both basic and industrial research fields for many decades. Palladium is remarkable in that it can absorb large quantities of hydrogen and hydrogen atoms are highly mobile in the Pd lattice. The phase diagram of $PdH_x$ exhibits a dilute $\alpha$-phase ($x < 0.02$ at 20°C) and a concentrated $\beta$-hydride ($0.6 \leq x \leq 1$ at 20°C) depending on the applied pressure. The $\alpha$-phase coexists with the $\beta$-phase below the critical point ($T_c \approx 300$°C, $P_c \approx 20$ bar) [1]. An increase in the lattice constant by 4 % accompanies the $\alpha$ to $\beta$ transformation, maintaining the crystal symmetry. The $\alpha$ to $\beta$ transition is highly reminiscent of a liquid-vapor phase transition.

There have been many attempts to elucidate the location and dynamics of hydrogen atoms in palladium lattice using neutron scattering techniques [2–29]. Neutron scattering has an advantage in that the scattering intensity from hydrogen is comparable to that from palladium, in sharp contrast to X-ray scattering. Another unique feature is that either coherent or incoherent scattering can be dominant depending on the extent to which it is deuterated. The coherent and incoherent bound atom neutron scattering cross sections for H, D, and Pd atoms are as follows; $\sigma_{coh}$(H) = 1.76 b, $\sigma_{inc}$(H) = 80.27 b, $\sigma_{coh}$(D) = 5.59 b, $\sigma_{inc}$(D) = 2.05 b, $\sigma_{coh}$(Pd) = 4.39 b, $\sigma_{inc}$(Pd) = 0.09 b, where b (barn) is equal to $10^{-24}$ cm$^2$ / atom. Deuterated materials, in which the coherent scattering is dominant, are commonly used for diffraction measurements and to investigate phonon dispersion relations. On the other hand the hydrogenated analogues, which have a huge contribution of incoherent scattering from H, are employed to measure the density of states of phonons and the self diffusion dynamics of H atoms.

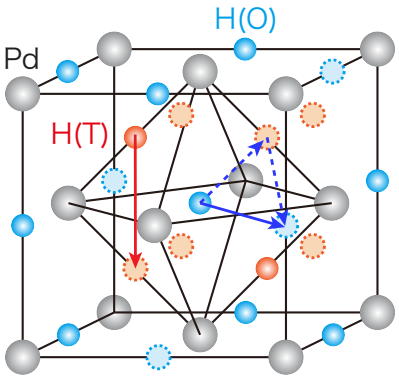


FIG. 1. (Color online) Possible hydrogen positions in the fcc palladium lattice; octahedral (O) sites $(1/2, 1/2, 1/2)$ and tetrahedral (T) sites $(1/4, 1/4, 1/4)$. The solid arrow represents a jump among adjacent O- (or T-) sites. The dashed arrows show a possible diffusion pathway for the O-site jump.

Neutron diffraction (ND) experiments have revealed that hydrogen atoms are accommodated at interstitial octahedral (O) sites $(1/2, 1/2, 1/2)$ in the face-centered cubic (fcc) lattice of Pd (see Fig. 1) at ambient temperature [2–12]. At temperatures as high as 300°C, hydrogen atoms can partially occupy tetrahedral (T) sites $(1/4, 1/4, 1/4)$ [9–12]. The stable O-sites and metastable T-sites in the Pd lattice are also predicted by *ab initio* calculations [30–32]. Below $T \approx 50$ K, at which tem-

* yamamuro@issp.u-tokyo.ac.jp

perature an anomaly is observed in the resistivity and heat capacity, additional diffraction peaks appear gradually with time, indicating a slow positional ordering of the hydrogen atoms [3, 5–10]. A recent heat capacity study attributed the anomaly to a glass transition corresponding to the freezing of the configurational motion of hydrogen, which occurs above a hypothetical order-disorder transition temperature [33].

The diffusion dynamics of hydrogen atoms has been examined using quasielastic neutron scattering (QENS) [13–18]. The QENS technique can provide space (1 Å to 100 Å) and time (1 ps to 100 ns) information on diffusion processes. These studies suggest that the diffusion occurs through jumps between adjacent O-sites, though some of the results quantitatively conflict with one another. The theoretical calculations indicate that the potential barrier is rather low for the diffusion path along ⟨111⟩ directions passing through T-sites (depicted by dashed arrows in Fig. 1) [30–32, 34–36]. As a consequence, the high mobility of the H atoms is realized in the Pd lattice.

The vibrational dynamics of $PdA_x$ (A = H, D, T) has been investigated via inelastic neutron scattering (INS) measurements [19–29]. In the $\beta$ phase, the oscillations of hydrogen atoms are described as optical phonons. The oscillation energy of the H atoms is ca. 60 meV which is consistent with calculations for the O-site occupation [30, 31]. Anharmonicity and anisotropy of phonon spectra have been pointed out [21, 24, 25, 28, 29]. The investigation of the optical phonons is significant also in understanding the inverse isotope effect of superconductivity in this system [37–39].

When metal particles are reduced to the nanometer-scale, their physicochemical properties differ significantly from those in bulk and strongly depend on their size [40–43]. Metal nanoparticles show promise as advanced materials with novel electronic, magnetic, optical, and catalytic properties. As for Pd nanoparticles, their properties were investigated by pressure composition isotherm (PCT) [44–47], heat capacity [33, 42], X-ray diffraction (XRD) [48–52], extended X-ray absorption fine structure (EXAFS) [53, 54], and neutron scattering measurements [55–58], inter alia. The PCT measurements for $PdH_x$ nanoparticles [44–47] demonstrated that the miscibility gap between the $\alpha$ and $\beta$ phases is narrowed on reducing the particle size; the higher absorption ability is achieved in the $\alpha$ phase but the $\beta$ phase is destabilized. Since surface effects are significant in nanoparticles with a large surface area, it indicates that the potential energy for hydrogen drastically changes near the surface. In fact, it has been pointed out that the sites in the subsurface (a few layers below the surface) region are more energetically favorable than those in the bulk [59–67]. However, the reason for the thermodynamic stability of the subsurface and the origin of the surface effects are not yet fully understood.

The particle size effect on the Pd lattice has been investigated by XRD and EXAFS measurements [48–54]. They also suggest the narrowing of the miscibility gap in the nanoparticles, which is detectable by the change in the lattice constant. It was also reported that the phase transformation from the fcc to an icosahedral structure occurs in nanoparticles as small as 2.5 nm [50, 53].

Most recently, Akiba and co-workers performed ND measurements for $PdD_{0.363}$ with a particle size of 8 nm [55]. Their Rietveld analysis revealed that a relatively large fraction ($\approx 31$ %) of hydrogen atoms occupy the T-sites even at $T = 300$ K. It was also shown that the T-site occupation occurs only in a limited area, probably the subsurface region, and its fraction decreases upon cooling. The results suggest that the T-sites are stabilized in the subsurface region though the O-sites are still more energetically favorable.

An INS study of $PdH_x$ ($x \leq 0.048$), with a particle size of less than 23 nm, was reported by Stuhr *et al.* [56, 57]. Excess vibrational excitations were observed in the energy region between 90 meV and 140 meV which is higher than the vibration energy of H atoms in bulk $PdH_x$. The excess excitations were interpreted as the vibrational states of H atoms in the subsurface and at the surface.

Janßen *et al.* have made QENS measurements for nanoparticles of $PdH_x$ ($x \approx 0.03$) [58]. They found a faster diffusion process with a smaller activation energy in the nanoparticles. The faster process was attributed to diffusion within the grain boundaries. This first QENS work was quite challenging, but the microscopic nature of the process was not well specified.

In the present article, we report QENS measurements on bulk $PdH_{0.73}$ and high quality nanocrystalline $PdH_{0.47}$. This is the first QENS work for concentrated $PdH_x$ nanocrystals. In order to explore the diffusion dynamics in a wide time range, several spectrometers with different energy resolutions and windows were used. The previous QENS work on bulk $PdH_x$ [13–17] was performed 40 years ago and the results quantitatively conflict with each other. The performance of neutron scattering spectrometers has been substantially improved in the past few decades. In particular, spectrometers with high energy resolution have been invented and constructed. The use of the modern sophisticated neutron spectrometers enables us to examine the diffusion of H atoms in bulk Pd more precisely.

The nanoparticles used by Janßen *et al.* adhered to one another and so hydrogen diffusion at the grain boundaries was mainly observed [58]. In addition, no information on the size and shape of the nanoparticles was given. We aim at investigating hydrogen diffusion *within* Pd nanoparticles. Our nanocrystals have a truncated cuboctahedron shape and have narrow size distribution ($8.0 \pm 0.9$ nm). The nanocrystals are covered with a protective polymer to avoid adhesion between the particles. Therefore no grain boundaries exist. The nanocrystals used in this work are basically the same as those used in the ND [55] and heat capacity [33] measurements. It is often discussed that the properties near the surface depend on

the shape of the particles, the surface facets, etc. Hence it is important to use the same samples as those for other measurements to have a rigorous discussion.

## II. EXPERIMENTAL

### A. Samples

A commercial reagent, Pd black, whose purity was reported to be better than 99.9 %, was purchased from Sigma Aldrich and used as a bulk sample. The powder was first annealed under vacuum at 100°C for 12 h to remove water and air adsorbed on the Pd surface. It was then hydrogenated under an atmosphere of $H_2$ gas (Suzuki Shokan Co. Ltd., 99.99 %) at 0.1 MPa and 20°C for 2 h. The hydrogen concentration was estimated to be $x = 0.728$ from the PCT curve reported in the literature [1].

Pd nanocrystals were grown in the same manner as described in Ref. 68. The nanocrystals have a well-defined shape of a truncated cuboctahedron with {111} and {100} facets and are of narrow size distribution (8.0± 0.9 nm) as characterized by transmission electron microscope measurements. In order to avoid adhesion between nanocrystals, they were covered with a protective polymer, polyvinylpyrrolidone (PVP). Two sets of Pd nanocrystals were prepared for QENS measurements at the HFBS and TOFTOF spectrometers (the descriptions of the spectrometers are given in Sec. II B). They are essentially the same shape and size but have different amounts of PVP. The ratios of Pd to PVP are 74.5 : 25.5 for the measurement at HFBS and 68 : 32 for TOFTOF, as determined by elemental analyses.

The following pretreatment was done because the low absorption ability of as-grown nanoparticles is often reported [69]. The nanocrystals were evacuated at 100°C for 1 h and exposed to a $H_2$ atmosphere of 0.1 MPa at 50°C for 1 h. These procedures were repeated several times. After the pretreatment, the nanocrystals were outgassed at 100°C for 12 h to completely remove hydrogen. Finally the hydrogenation was carried out at 0.1 MPa and 23°C for 2 to 3 days because it took a long time to obtain an equilibrium state for the hydrogenation of nanocrystals. The concentrations were determined from the reduction in pressure of the gas handling system. The obtained values were $x = 0.52$ for HFBS and $x = 0.42$ for TOFTOF. The values are roughly consistent with those evaluated from the previous PCT curve [45]. The averaged value ($x = 0.47$) is hereafter referred to as the concentration of the nanocrystals in the present work.

The bulk and nanocrystalline $PdH_x$ were loaded into concentric double-cylinder Al cells with $H_2$ gas. The outer diameter of the cell was 18 mm and the thickness of the sample confined between the two Al walls was 0.5 mm to 1 mm, giving a neutron transmission > 85 %, in order to reduce multiple scattering effects. The amounts of sample used were 5.88 g for (bulk $PdH_{0.73}$), 1.30 g (nano $PdH_{0.52}$ with PVP), and 2.01 g (nano $PdH_{0.42}$ with PVP). The sample cells were sealed using indium or lead gaskets.

### B. Quasielastic neutron scattering

The bulk $PdH_{0.73}$ was measured using three spectrometers at the NIST Center for Neutron Research (NCNR) of the National Institute of Standards and Technology (NIST) in the USA; a backscattering spectrometer HFBS [70], a disk chopper time-of-flight spectrometer DCS [71], and a neutron spin echo spectrometer NSE [72, 73]. The measurements on the nanocrystalline $PdH_{0.47}$ were conducted at the HFBS and at the time-of flight spectrometer TOFTOF [74, 75], operated by Technische Universität München, at Forschungsneutronenquelle Heinz Maier-Leibnitz (FRM II) in Germany.

HFBS [70] is a high flux backscattering spectrometer with a high energy resolution. The flux of the incident neutrons is enhanced by the phase space transform (PST) chopper. The incident neutrons are Doppler shifted by the oscillating Si(111) monochromator, providing a band centered at 2.08 meV. The scattered neutrons with the energy of 2.08 meV are selected by multiple Si(111) analyzers and counted using 16 $^3$He detectors. The high energy resolution is realized owing to the backscattering condition of Si(111) monochromator/analyzer with good crystallinity. In the experiments for both bulk and nanocrystalline $PdH_x$, we used an energy window, -15 $\mu$eV $\leq \hbar\omega \leq$ 15 $\mu$eV, set by the chosen Doppler frequency. The energy resolution was $\Delta E = 0.8$ $\mu$eV (full width at half maximum), which enables us to investigate the relaxation in a time range between 100 ps and 5 ns. The $Q$-range covered by HFBS was 0.25 Å$^{-1}$ $\leq Q \leq$ 1.75 Å$^{-1}$. QENS spectra were recorded at $T$ = (50, 230, 260, 300, 340) K for the bulk sample and at $T$ = (4, 150, 170, 200, 250, 300) K for the nanocrystals. The data at the lowest temperature were used as the instrumental resolution.

DCS [71] is a time-of-flight spectrometer with a tunable energy window and resolution. A pulsed monochromatic beam with an energy of $E_\mathrm{i}$ is produced by two pairs of disk choppers and scattered by the sample. Time-of-flight analysis of events in a large array of detectors determines an energy transfer $\hbar\omega$ and a wave vector transfer $Q$. Each chopper has three slots of different width, corresponding to low, medium, and high resolution conditions. Additional choppers are employed to remove higher orders and to minimize frame overlap. Measurements of the bulk $PdH_{0.73}$ were carried out using incident neutron energies $E_\mathrm{i}$ of 2.13 meV with the low resolution slots and 5.38 meV with the medium resolution slots. The corresponding energy resolution was $\Delta E = 58$ $\mu$eV and $\Delta E = 100$ $\mu$eV, respectively. The accessible energy and $Q$-range at the elastic position were -2 meV $\leq \hbar\omega \leq$ 1.2 meV and 0.09 Å$^{-1}$ $\leq Q \leq$ 1.91 Å$^{-1}$

($E_\mathrm{i}$ = 2.13 meV) and -4 meV $\leq \hbar\omega \leq$ 2.5 meV and 0.14 Å$^{-1} \leq Q \leq$ 3.03 Å$^{-1}$ ($E_\mathrm{i}$ = 5.38 meV). The time window in these conditions is roughly from 1 ps to 100 ps. The condition with $E_\mathrm{i}$ = 5.38 meV was used to determine the jump length of the diffusion process as shown later. QENS spectra were recorded at $T$ = (40, 230, 260, 300, 340, 390) K with $E_\mathrm{i}$ = 2.13 meV, and $T$ = (40, 230, 450) K with $E_\mathrm{i}$ = 5.38 meV. The data at 40 K were used as the instrumental resolution.

TOFTOF [74, 75] is also a time-of-flight spectrometer similar to DCS in many respects. In the measurements of nanocrystalline PdH$_x$, the incident energy of 0.57 meV was chosen. The intense beam at TOFTOF is beneficial for exploring a weak scattering signal in the nanocrystalline sample. The corresponding energy resolution, energy window, and $Q$-range were $\Delta E$ = 8.1 $\mu$eV, $-200$ $\mu$eV $\leq \hbar\omega \leq$ 200 $\mu$eV and 0.05 Å$^{-1} \leq Q \leq$ 0.95 Å$^{-1}$, respectively. The time range covered is between 10 ps and 1 ns. The data were collected at $T$ = (10, 260, 300, 340) K. The data at 10 K were used as the instrumental resolution.

NSE [72, 73] is a special instrument with the highest energy resolution among neutron spectrometers, in spite of the fact that the incident neutron beam has a broad wavelength distribution. NSE works in the time domain, being advantageous for detecting slow relaxation phenomena, in contrast to ordinary energy domain spectrometers including those described above. Larmor precession of the neutron's spin is exploited in the NSE technique. Relaxation phenomena are observable by measuring the change in the precession phase, which is detected by polarization analyses, before and after the scattering. The incident wavelength of neutrons used was 6 Å with the wavelength resolution of about 20 %. The data were collected at Fourier times between 0.007 ns and 15 ns. The spin echo measurements were made at $Q$ = 0.8 Å$^{-1}$ and $T$ = (25, 185, 205, 230, 260, 300) K. The data at 25 K were used as the instrumental resolution.

The raw data obtained at HFBS, DCS, and NSE were reduced using the DAVE software package [76] and those at TOFTOF using Mantid [77].

## III. RESULTS AND DISCUSSION

### A. Bulk PdH$_x$

The QENS measurements on bulk PdH$_{0.73}$ were performed using the three spectrometers, NSE, HFBS, and DCS, in order to explore diffusion dynamics of H atoms over a wide time range. Figure 2(a) shows the normalized intermediate scattering functions $I(Q,t)/I(Q,0)$ at $Q$ = 0.8 Å$^{-1}$ measured on the NSE spectrometer. $I(Q,t)/I(Q,0)$ decays more rapidly as the temperature is increased, as expected. We initially attempted to fit the data with a single exponential as in previous work [13–17]. However, the fits were not satisfactory at the higher temperatures ($T \geq$ 230 K). The data were then fitted

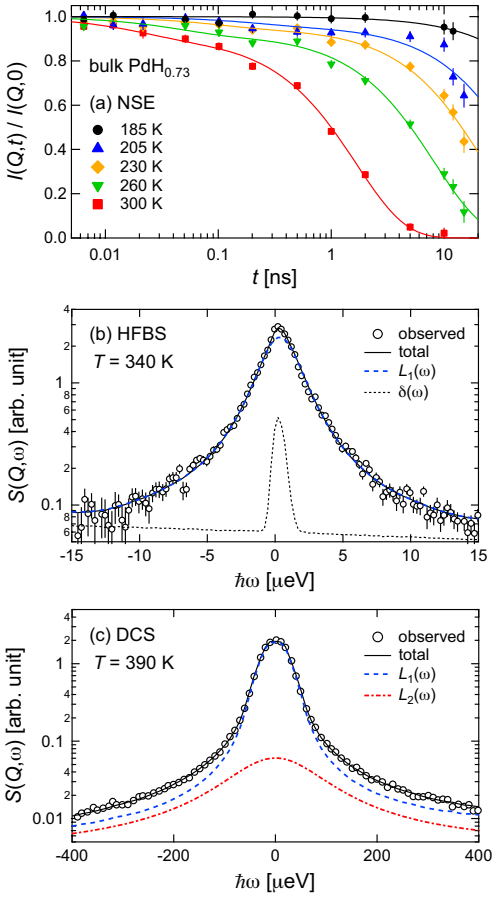


FIG. 2. (Color online) (a) Intermediate scattering functions and (b)(c) dynamic structure factors of bulk PdH$_{0.73}$ observed at $Q$ = 0.8 Å$^{-1}$. The data are taken on the (a) NSE, (b) HFBS, and (c) DCS spectrometers. Error bars throughout this article represent one standard deviation. The curves are the results of the fitting. See the text for details.

with two exponential functions:

$$\frac{I(Q,t)}{I(Q,0)} = (1-f)\exp\left(-t/\tau_1\right) + f\exp\left(-t/\tau_2\right), \qquad (1)$$

where $\tau_1$ and $\tau_2$ are relaxation times ($\tau_1 > \tau_2$) and $f$ the fraction of the fast motion. The results are good, as shown by the solid curves in Fig. 2(a). In the final analysis, $\tau_2$ was fixed to the value extrapolated from the DCS data in which $\tau_2$ can be well determined, assuming that the temperature dependence of $\tau_2$ is of Arrhenius type. This procedure is effective to estimate the parameter $f$ appropriately.

The dynamical structure factors $S(Q,\omega)$ taken on HFBS and DCS are presented in Fig. 2(b) and (c), respectively. Clear QENS spectra with broad symmetric peaks were observed. The QENS spectra taken on HFBS were fitted to the function,

$$S(Q,\omega) = R(Q,\omega) \otimes [A_\mathrm{E}\delta(\omega) + A_1 L_1(Q,\omega)] + \mathrm{BG}. \qquad (2)$$

On the other hand, the following function was used to

reproduce the spectra measured on DCS;

$$S(Q,\omega) = R(Q,\omega) \otimes [A_1 L_1(Q,\omega) + A_2 L_2(Q,\omega)] + \mathrm{BG}. \quad (3)$$

$L_1(Q,\omega)$ and $L_2(Q,\omega)$ are Lorentz functions described as

$$L_i(Q,\omega) = \frac{1}{\pi} \frac{\Gamma_i(Q)}{\omega^2 + \Gamma_i(Q)^2}, \quad (4)$$

where $\Gamma_i(Q)$ is the half width at half maximum (HWHM) of the function and inversely proportional to the relaxation time ($\Gamma = 1/\tau$). In Eq. (2) and (3), $R(Q,\omega)$ represents the resolution function of the spectrometer, $\delta(\omega)$ the delta function, $\otimes$ the convolution operator, and BG a linear background. $A_\mathrm{E}$, $A_1$, and $A_2$ represent the areas of the elastic peak, the narrower Lorentzian, and the wider Lorentzian, respectively. The fitting procedures for all $S(Q,\omega)$ data were carried out using the PAN program in the DAVE software package. The results of the fits are shown by solid curves in Fig. 2(b) and (c). The small contribution from the elastic component (4 %) in the HFBS data could be due to the background from the cell and the instrument.

It should be noted here that only motions matching the time scale of the instrument are detectable. In fact, the fast relaxation ($L_2$) is much faster than the time scale of HFBS (0.1 ns to 5 ns) and so its quasielastic line is too broad, merging with a flat background. On the other hand, the slow relaxation is too slow for DCS below 340 K and $L_1$ was replaced by a delta function.

It is helpful to look at the $Q$-dependence of the HWHM ($\Gamma_i$) of the QENS spectra, in order to trace the origins of the two relaxation processes. In the jump diffusion model proposed by Chudley and Elliott (CE) [78], the diffusion process consists of a sequence of elementary jumps of atoms into adjacent vacant sites. Here it is assumed that the jumps are instantaneous, uncorrelated, and independent of other kinds of motions such as vibrations. For powder samples, the model can be written as

$$\Gamma(Q) = \frac{1}{\tau_\mathrm{r}} \left(1 - \frac{\sin Ql}{Ql}\right), \quad (5)$$

where $\tau_\mathrm{r}$ refers to the mean residence time at a site and $l$ is a jump length. In the low-$Q$ region, $\Gamma(Q)$ is approximately equal to $DQ^2$, where $D$ ($=l^2/6\tau_\mathrm{r}$) is the self-diffusion coefficient. Figure 3 displays the peak widths $\Gamma_1$ (for the slow process), and $\Gamma_2$, as functions of $Q$. $\Gamma_1(Q)$ was determined from the data taken on HFBS and $\Gamma_2(Q)$ from the data on DCS with $E_\mathrm{i} = 5.38$ meV which permits investigation over a wide $Q$-range. Both $\Gamma_1(Q)$ and $\Gamma_2(Q)$ were well described by the CE model with a jump length of 2.85 Å which corresponds to the distance between the adjacent O-sites, as shown by the solid curves in the plots. The calculated values assuming jumps between the T-sites ($l = 2.02$ Å) do not reproduce the experimental data.

Figure 4 shows the fraction of the fast component, $f = A_2/(A_1 + A_2)$, as a function of temperature. It is evident

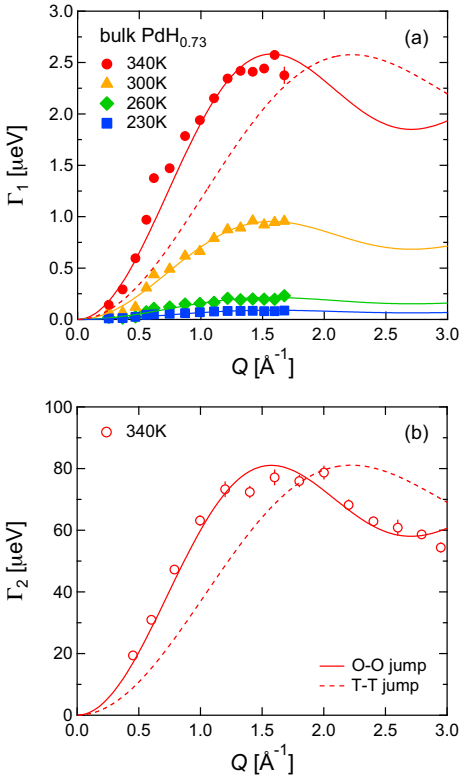


FIG. 3. (Color online) $Q$-dependence of HWHM for (a) the slow process ($\Gamma_1$) measured on HFBS and (b) the fast one ($\Gamma_2$) on DCS in bulk $PdH_{0.73}$. Solid curves are the results of the fit based on the CE model (see Eq. (5)) for the O-O jumps. Calculated values for the T-T jumps are also presented as dashed curves for comparison.

that $f$ decreases upon cooling, indicating that the fast jump process originates in the jump of H atoms in an excited state. Given that the population of the excited state follows the Boltzmann distribution, the fraction $f$ can be expressed as

$$f = \frac{\exp(-\Delta/k_\mathrm{B}T)}{1 + \exp(-\Delta/k_\mathrm{B}T)}. \quad (6)$$

The solid curve in Fig. 4 represents the result of the fit using this equation. The energy difference between the ground and excited states was estimated to be $\Delta = (62.4 \pm 2.8)$ meV. A discussion about the value of $\Delta$ is given later.

Figure 5 presents the relaxation times at $Q = 0.8$ Å$^{-1}$ plotted against reciprocal temperature (an Arrhenius plot), together with previous QENS data by Beg *et al.* [14] for $PdH_{0.65}$ and Nelin *et al.* [17] for $PdH_x$ ($x = 0.4$ to 0.48). Their data were converted to values at $Q = 0.8$ Å$^{-1}$ for purposes of comparison. Relaxation times obtained from nuclear magnetic resonance (NMR) experiments for $PdH_{0.7}$ are also shown. It was pointed out that there was a discrepancy in the $T$-dependence of the relaxation time between the previous QENS [14] and NMR data [79]. As seen in Fig. 5, our QENS data

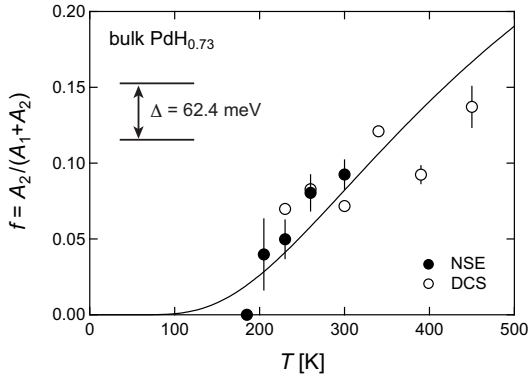


FIG. 4. Temperature dependence of the fraction of the fast relaxation $f = A_2/(A_1+A_2)$ at $Q = 0.8$ Å$^{-1}$ determined from the measurements on NSE and DCS. The solid curve presents the result of the fit assuming the Boltzmann distribution for a two level system (see Eq. (6)).

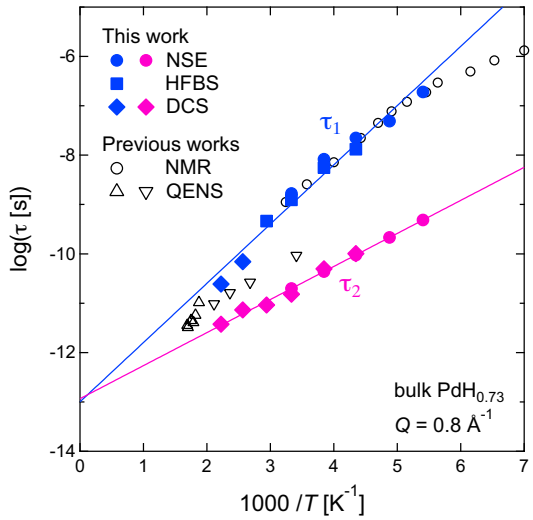


FIG. 5. (Color online) Arrhenius plots of the relaxation times for the slow ($\tau_1$) and fast ($\tau_2$) diffusion processes observed in bulk $PdH_{0.73}$. The plotted data are the values at $Q = 0.8$ Å$^{-1}$. The solid lines represent the results of the fit assuming the Arrhenius law (Eq. (7)). The previous QENS data by Beg *et al.* [14] ($\bigtriangledown$) and Nelin *et al.* [17] ($\bigtriangleup$) and NMR data [79] ($\bigcirc$) are also plotted.

are now in good agreement with the NMR data. In the previous QENS studies, the fast process was not recognized and the spectra were fitted with a single Lorentz function; the analysis assuming two components might be difficult for the low quality data taken 40 years ago. The previous QENS data are located in an area between the slow and fast processes observed in this work. This often happens when oversimplified models are used for the fitting.

The activation energies, $E$, for the two diffusion processes were estimated from the fits with the Arrhenius

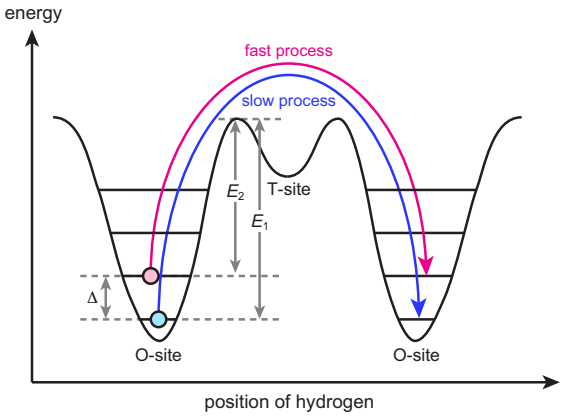


FIG. 6. (Color online) Schematic drawing of the potential energy against the position of a hydrogen atom along the O-T-O direction (dashed arrows in Fig. 1) for bulk $PdH_x$. $E_1$ and $E_2$ are the activation energies for the slow and fast processes. $\Delta$ is the energy difference between the ground and first excited states.

equation,

$$\tau = \tau_0 \exp\left(-E/k_{\rm B}T\right), \qquad (7)$$

where $\tau_0$ denotes the relaxation time in the high temperature limit. The results of the fits are presented as solid lines in Fig. 5. The activation energies evaluated for the slow and fast processes are $E_1 = (238.1 \pm 13.9)$ meV and $E_2 = (132.9 \pm 9.5)$ meV, respectively. The value of $E_1$ is almost the same as $E = 228$ meV [79] estimated from the NMR data in the range 195 K $< T <$ 330 K where the slow process is dominant. It should also be mentioned that the major slow relaxation deviates from the Arrhenius law at low temperatures, suggesting a tunneling effect in the diffusion mechanism, such as phonon assisted tunneling [80].

From the Arrhenius fits, $\tau_0$ was estimated to be $1.0 \times 10^{-13}$ s and $1.2 \times 10^{-13}$ s for the slow and fast processes, respectively. These times are nearly the same as the reciprocal frequency of optical phonon ($6.5 \times 10^{-14}$ s) [25]. It should be noted that the jump rate, $\tau^{-1}$, depends on the number of vacancies; the probability of finding vacant sites becomes lower at high H concentrations. This decreases the "effective" jumping rate by a factor of 3 to 4 for $x = 0.73$. Self-trapping [31] and non-adiabatic [36] effects, which could be significant for H diffusion in Pd, also influence the jump rate. Furthermore, the H-H correlation effect can cause non-Debye relaxation behavior. Despite this effect, our QENS data were well described by the Lorentz function which is the Fourier transformation of the Debye relaxation function. We speculate that this effect is less significant at high temperatures.

We now consider the origins of two jump processes among the O-sites. Figure 6 shows a schematic drawing of the potential energy surface for the position of hydrogen atoms along the O-T-O direction (corresponding to the dashed arrows in Fig. 1). As mentioned in Sec. I, the

potential energy at a saddle point between the O and T sites is significantly lower than those at positions along other directions [30–32, 34–36]. Hence, the H atoms diffuse preferentially through the saddle point, along the O-T-O pathway.

The energy difference between the O-site and the saddle point corresponds to the energy barrier for hydrogen diffusion in a classical picture. The ab initio calculations, taking account of the relaxation of the Pd host lattice, predicted that the energy barrier is (200 to 250) meV [30, 31]. The activation energy for the observed major diffusion ($E_1 = 238$ meV) is in reasonable agreement with the calculated energy barrier. It is mentioned that the energy barrier can also be marginally modified by the self-trapping and non-adiabatic effects.

The fast diffusion process apparent at higher temperatures is attributable to the motion of the hydrogen atoms populated at the first excited state. The fast diffusion takes place along the same O-T-O path. As shown in Fig. 4, the energy gap between the ground and first excited states was estimated to be $\Delta = 62.4$ meV which approximately corresponds to the vibrational energy of H atoms (63.7 meV) [25]. In terms of the activation energy of the fast process $E_2$, the relation $E_2 = E_1 - \Delta$ should be satisfied according to our scenario. The experimental value of $E_2$ of 133 meV is more or less consistent with $E_1 - \Delta = 175$ meV.

Finally, we comment on the two-state model for $NbH_x$ proposed by Lottner *et al.* [81]. The model, in which a transition rate between a trap site and a mobile site was introduced, predicted a complicated single process. The key difference between the model and our model is the ratio between the two characteristic rates. Our model supposes that the transition rate between the ground and the excited states (the inverse of the lifetime of the excited state) is much smaller than the relaxation rate and so the H diffusion process can be treated as two relaxation processes. If the transition rate is comparable to the relaxation rate, two relaxation processes cannot be resolved and a single relaxation process could be observed. Schimmele *et al.* have discussed this scheme and the effect of excited states on the relaxation process in NMR data of metal hydrides [82]. For $PdH_x$, it is difficult to evaluate the real lifetime from the linewidth of the phonon spectra because of strong anharmonicity and dispersion relation. However, our assertion of the long lifetime could be justified by the fact that the $Q$-dependence of the relaxation times was well described by the CE model (Fig. 3). In the two-state model by Lottner *et al.*, the process exhibits a complicated $Q$-dependence of the relaxation time. It is possible that such a complicated process is observed at higher temperatures in $PdH_x$.

### B. nanocrystalline $PdH_x$

Figure 7 shows QENS spectra taken on HFBS and TOFTOF at $Q = 0.8$ Å$^{-1}$ for nanocrystalline $PdH_{0.47}$.

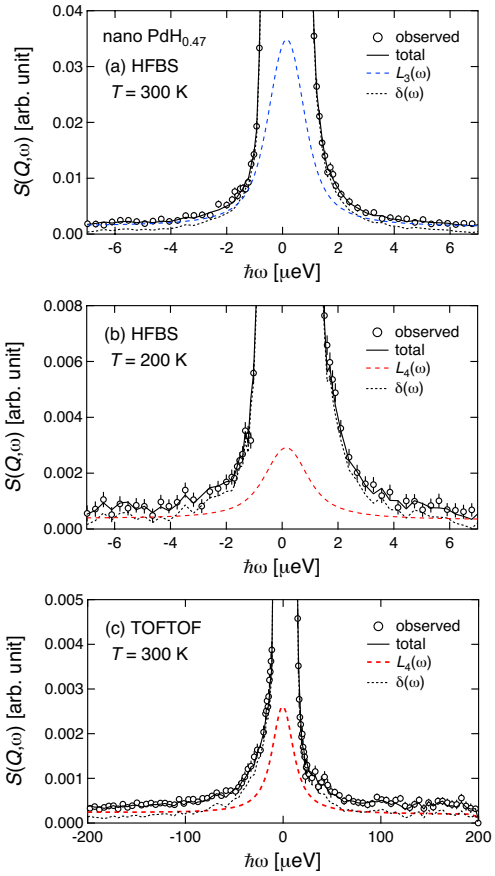


FIG. 7. (Color online) Dynamic structure factors of nanocrystalline $PdH_{0.47}$ observed at $Q = 0.8$ Å$^{-1}$, taken on the (a)(b) HFBS and (c) TOFTOF spectrometers. The curves are the results of the fitting. See the text for details.

Here the values at $\hbar\omega = 0$ are scaled to 1. Solid curves represent the results of fits using the sum of a delta and a Lorentz functions,

$$S(Q,\omega) = R(Q,\omega) \otimes [A_{\rm E}\delta(\omega) + A_i L_i(Q,\omega)] + {\rm BG}, \quad i = 3 \text{ or } 4 \tag{8}$$

The definitions of the functions and parameters are identical to those in Eq. (2), (3), and (4). In the HFBS data, the line widths at 200 K and 300 K are comparable, but the intensity at 200 K is much weaker than that at 300 K (see Fig. 7(a)(b)). It suggests that the relaxation observed at 200 K significantly differs from that at 300 K. We assign the two relaxation components as $L_3$ (slow relaxation) and $L_4$, respectively. The spectrum taken on TOFTOF at 300 K also exhibit a weak QENS component corresponding to the fast relaxation ($L_4$). It should be emphasized that weak QENS signals were successfully observed on both the spectrometers, though there exist strong elastic signals from the H atoms present in PVP. It is also noted that no QENS broadening was detected in the measurements for PVP only, indicating that the H atoms in PVP are immobile in the energy range investigated.

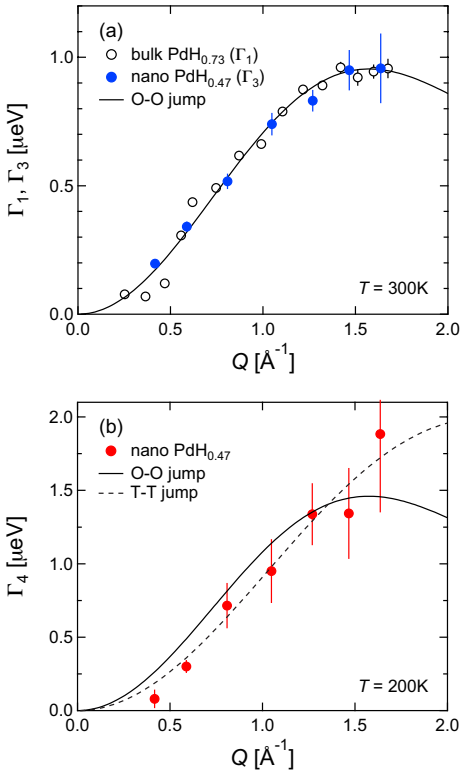


FIG. 8. (Color online) $Q$-dependence of HWHM for (a) the slow process ($\Gamma_3$) at 300 K and (b) the fast one ($\Gamma_4$) at 200 K in nanocrystalline $PdH_{0.47}$. The HWHM were evaluated by fitting the data taken on HFBS. The solid and dashed curves are the results of the fit based on the CE model (Eq. (5)) assuming the O-O and T-T jumps, respectively.

The peak widths ($\Gamma_3$, $\Gamma_4$) are plotted as a function of $Q$ in Fig. 8. The data were analyzed using the CE model (Eq. (5)) in the same manner as the bulk sample. As can be seen, $\Gamma_3$ is in excellent agreement with that for the slow process ($\Gamma_1$) in bulk. Therefore, the slow process in nanocrystalline $PdH_x$ is identified as jump diffusion between adjacent O-sites. On the other hand, the fast process can be reproduced using both O-site jumps and T-site jumps. The origin of the fast process is discussed later.

Figure 9 displays the temperature dependence of the fractions of the slow and fast relaxation. Each fraction is defined with reference to the elastic signal,

$$f_3 = \frac{A_3}{A_E + A_3}, \tag{9}$$

$$f_4 = \frac{A_4}{A_E + A_4}, \tag{10}$$

which is different from the definition of $f$ for the bulk sample. As stated above, $A_E$ results from the immobile H atoms in PVP. Care was taken to correct the difference in the quantity of PVP between two sets of nanocrystalline samples measured on HFBS and TOFTOF.

When the temperature is raised, the fraction of the slow process $f_3$ reduces and that of the fast one $f_4$ increases. It indicates that the fast process is the motion of the H atom in a metastable state. The data is reminiscent of the fast process observed in bulk $PdH_{0.73}$ (the O-site jump between excited states). However, the fast process observed in the nanocrystals is not identical to that in bulk. In fact, the fast process is more pronounced in the nanocrystals; the ratio between the two components, [fast]/[slow], is (0.143 ± 0.031) for the nanocrystals and (0.075 ± 0.001) for the bulk at $T \approx 250$ K. Moreover, there is a clear difference in the relaxation times of the fast processes between the nanocrystalline and bulk samples ($\tau_2$, $\tau_4$), as seen in Fig. 10. In contrast, the slow process in the nanocrystals ($\tau_3$) is nearly identical to that in the bulk sample ($\tau_1$). Hence we argue that the fast process ($\tau_4$) is the H motion that is newly appeared in nanocrystalline $PdH_{0.47}$. The activation energy for the fast relaxation, $E_4$, was estimated to be (120.3±3.2) meV from the Arrhenius fit (Eq. (7)).

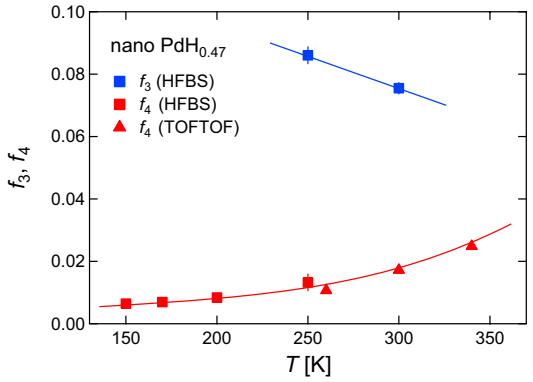


FIG. 9. (Color online) Temperature dependence of the fraction of the slow ($f_3$) and fast relaxation ($f_4$) at $Q = 0.8$ Å$^{-1}$. Solid curves are the guide to the eye.

The major findings for the hydrogen diffusion in nanocrystalline $PdH_x$ are summarized as follows. (i) Two distinct diffusion processes are present. (ii) The slow process closely resembles that observed in the bulk (diffusion between O-sites). (iii) The fast process with a smaller activation energy, which is not identical to the fast motion in bulk, becomes more prominent at high temperatures. The jump length of the process remains obscure due to the lack of high-$Q$ data. Further work will make it clear whether the H atoms diffuse on the T- or O-sites.

It should be mentioned that the fast process found in this work is essentially different from that of the $PdH_x$ nanoparticles in the low concentration regime ($x \approx 0.03$), reported by Janßen et al [58]. As compared to our data, Janßen's relaxation time is an order of magnitude shorter and the activation energy is 2 to 3 times smaller. The faster relaxation process is interpreted as H diffusion within the grain boundaries. In our nanoparticles, capped by PVP, where no grain boundary exists, such a faster process was not detected. The relaxation processes detected in this work are indeed H motions *within* the nanoparticle.

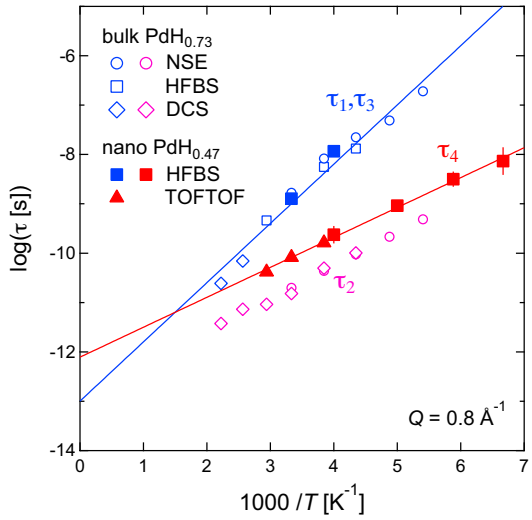


FIG. 10. (Color online) Arrhenius plots of the relaxation times for the hydrogen motions in nanocrystalline $PdH_{0.47}$ and bulk $PdH_{0.73}$. All of the plotted data are the values at $Q = 0.8$ Å$^{-1}$. The solid lines represent the results of the fits with assuming the Arrhenius law (Eq. (7)).

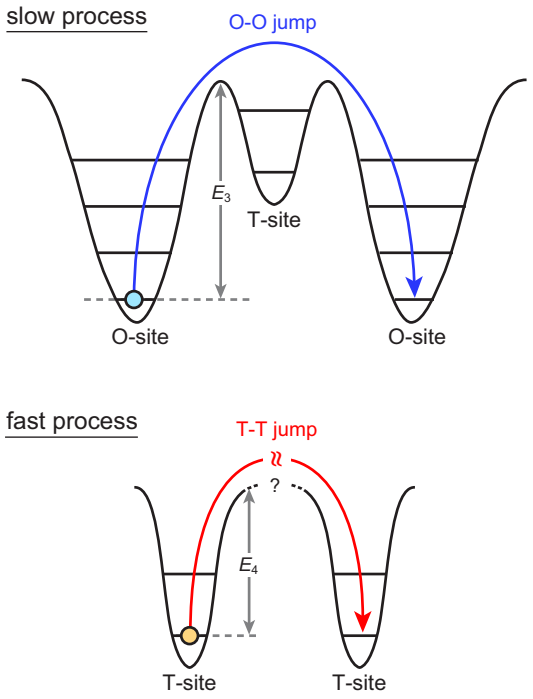


FIG. 11. (Color online) Possible mechanism for the two diffusion processes in nanocrystalline $PdH_x$. $E_3$ and $E_4$ are the activation energies for the slow and fast processes. See the text for details.

It has been considered that the potential energy at hydrogen sites drastically changes in the subsurface region, as mentioned in Sec. I. It is thus likely that the new fast process arises from the hydrogen atoms in this region. The lattice constant of the Pd nanoparticles is larger than that of the bulk sample [45, 49, 55], contrary to other metals. It implies that the Pd lattice expands near the surface. Density functional theory (DFT) calculations indicated that both the energy barrier for diffusion and the difference of the energy between the O- and T-sites become small for tensile strain [83]. Further, the molecular dynamics (MD) simulations for $PdH_x$ nanoclusters demonstrated that the activation energy becomes lower as the cluster size is reduced due to the less dense and softened Pd lattice in the outer parts of nanoparticles [84]. Not only a uniform strain but also a local distortion can play an important role in the potential energy near the surface of nanocrystals. Such strain and distortion presumably affect the relative stability of interstitial hydrogen sites. Indeed, recent ND work suggests that the D atoms partially occupy the T-sites in a limited area, probably the subsurface region [55].

On the basis of the experimental results, we discuss the mechanism for the diffusion processes observed in nanocrystalline $PdH_{0.47}$. The potential energy at the hydrogen sites appears rather inhomogeneous in the nanocrystal. The potential surface in the interior region, which is less disturbed by the surface effects, is similar to that in bulk (see Fig. 6). In the vicinity of the surface, the T-sites are stabilized due to surface effects, though O-sites are still more favorable. The *average* potential energy around the O-sites is depicted in the top panel of Fig. 11. Our QENS analyses demonstrated that the slow process closely resembles the O-site jumps observed in bulk. Therefore the slow process is jump diffusion along the the O-T-O pathway, which predominantly occurs in the interior region.

On the other hand, it is inferred that the fast process is H diffusion in the subsurface region. It is worth noting that the $T$-dependence of $f_4$ (fraction of the fast diffusion) is consistent with the experimental observation that the T-sites occupancy decreases upon cooling [55]. The possibility is thus raised that the fast process is a jump process between the T-sites (see the bottom figure of Fig. 11). With regard to the diffusion pathway, we preclude that the H atoms at the T-sites diffuse along the T-O-T direction, because the T-O-T jump process is indistinguishable from the O-T-O process. Another feasible diffusion pathway should be considered, for instance, the direct T-T or the indirect T-S-S-T (S : saddle point) path. We expect that the local distortion of Pd lattice near the surface creates such a new diffusion passage with a relatively low energy barrier. It is noted that the actual H motion in the vicinity of the surface might be described as a mixture of O- and T-site jump processes, which is beyond the framework of the CE model. The analysis based on such a complicated stochastic process requires experimental data with higher quality in a wider $Q$ region.

## IV. CONCLUSION

We have investigated diffusion dynamics of hydrogen in bulk and nanocrystalline palladium using the quasielastic neutron scattering technique. In bulk $PdH_{0.73}$, two diffusion processes were clearly observed. Both processes were well described by the jump diffusion (Chudley-Elliott) model involving instantaneous jumps among octahedral (O) interstitial sites. The fast O-site jump process disappears at low temperature ($T < 200$ K), indicating that it is due to the hydrogen in a thermally populated state. By comparing the activation energies for the diffusion processes and the energy gap between the ground and excited states, we conclude that the slow relaxation corresponds to a jump process between the ground states while the fast one is between the first excited states.

As for the $PdH_{0.47}$ nanocrystals with a size of 8 nm, we also found two types of diffusion processes. The slow process is almost identical to the O-site jump motion observed in bulk. This slow process is mainly attributed to the H atoms in the interior region of the nanocrystal which is hardly influenced by surface effects. On the other hand, the new fast process, which differs from the fast process in the bulk, is interpreted as the diffusion of hydrogen in the subsurface region. The recent neutron diffraction work on nanoparticles $PdD_x$ suggests that some of the hydrogen is accommodated at tetrahedral (T) sites. The fast relaxation process was more pronounced at higher temperatures, which is consistent with the temperature dependence of the T-site occupancy. It seems plausible that the fast process is jump diffusion between the T-sites in the subsurface. However since the jump length of the process remains obscure due to the lack of high-$Q$ data, our results are inconclusive with respect to the origin of the fast process. Further experimental and theoretical studies are needed to make a definitive conclusion on the diffusion mechanism and the site preference of H atoms in the subsurface.

## ACKNOWLEDGMENTS

We are grateful to M. Nagao for technical support during the experiments on NSE at the NCNR. This work was supported by Core Research for Evolutional Science and Technology (CREST) from Japan Science and Technology Agency (JST). The experiments at NCNR were financially supported by General User Program for Neutron Scattering Experiments, Institute for Solid State Physics, The University of Tokyo. This work utilized facilities supported in part by the National Science Foundation under Agreement No. DMR-1508249. Certain commercial equipment, instruments, or materials are identified in this paper to foster understanding. Such identification does not imply recommendation or endorsement by the National Institute of Standards and Technology, nor does it imply that the materials or equipment identified are necessarily the best available for the purpose.

[1] H. Frieske and E. Wicke, Ber. Bunsenges. Phys. Chem. **77**, 48 (1973).
[2] J. E. Worsham, M. K. Wilkinson, and C. G. Shull, J. Phys. Chem. Solids **3**, 303 (1957).
[3] G. A. Ferguson, A. J. Schindler, T. Tanaka, and T. Morita, Phys. Rev. **137**, A483 (1965).
[4] G. Nelin, Phys. Stat. Sol. **45**, 527 (1971).
[5] I. S. Anderson, C. J. Carlile, and D. K. Ross, J. Phys. C **11**, L381 (1978).
[6] O. Blaschko, R. Klemencic, P. Weinzierl, and O. Eder, Solid State Commun. **27**, 1149 (1978).
[7] T. E. Ellis, C. B. Satterthwaite, M. H. Mueller, and T. O. Brun, Phys. Rev. Lett. **42**, 456 (1979).
[8] O. Blaschko, R. Klemencic, P. Weinzierl, and O. Eder, Acta Cryst. **A36**, 605 (1980).
[9] S. J. Kennedy, E.Wu, E. H. Kisi, E. M. Gray, and B. J. Kennedy, J. Phys.: Condens. Matter **7**, L33 (1995).
[10] E. Wu, S. J. Kennedy, E. M. Gray, and E. H. Kisi, J. Phys.: Condens. Matter **8**, 2807 (1996).
[11] M. Pitt and E. M. Gray, Europhys. Lett. **64**, 344 (2003).
[12] K. G. McLennan, E. M. Gray, and J. F. Dobson, Phys. Rev. B **78**, 014104 (2008).
[13] K. Sköld and G. Nelin, J. Phys. Chem. Solids **28**, 2369 (1967).
[14] M. M. Beg and D. K. Ross, J. Phys. C **3**, 2487 (1970).
[15] J. M. Rowe, J. J. Rush, L. A. de Graaf, and G. A. Ferguson, Phys. Rev. Lett. **29**, 1250 (1972).
[16] C. J. Carlile and D. K. Ross, Solid State Commun. **15**, 1923 (1974).
[17] G. Nelin and K. Sköld, J. Phys. Chem. Solids **36**, 1175 (1975).
[18] B. J. Heuser, D. R. Trinkle, N. Jalarvo, J. Serio, E. J. Schiavone, E. Mamontov, and M. Tyagi, Phys. Rev. Lett. **113**, 025504 (2014).
[19] J. Bergsma and J. A. Goedkoop, Physica (Amsterdam) **26**, 744 (1960)
[20] M. R. Chowdhury and D. K. Ross, Solid State Commun. **13**, 229 (1973).
[21] J. M. Rowe, J. J. Rush, H. G. Smith, M. Mostoller, and H. E. Flotow, Phys. Rev. Lett. **33**, 1297 (1974).
[22] A. Rahman, K. Sköld, C. Pelizzari, S. K. Sinha, and H. Flotow, Phys. Rev. B **14**, 3630 (1976).
[23] W. Drexel, A. Murani, D. Tocchetti, W. Kley, I. Sosnowska, and D. K. Ross, J. Phys. Chem. Solids **37**, 1135 (1976).
[24] J. J. Rush, J. M. Rowe, and D. Richter, Z. Phys. B **55**, 283 (1984).
[25] J. M. Rowe, J. J. Rush, J. E. Schirber, and J. M. Mintz, Phys. Rev. Lett. **57**, 2955 (1986).
[26] A. I. Kolesnikov, I. Natkaniec, V. E. Antonov, I. T. Belash , V. K. Fedotov, J. Krawczyk, J. Mayer, and E. G. Ponyatovsky, Physca B **174**, 257 (1991).
[27] Y. Nakai, E. Akiba, H. Asano, and S. Ikeda, J. Phys. Soc. Jpn. **61**, 1834 (1992).

[28] D. K. Ross, V. E. Antonov, E. L. Bokhenkov, A. I. Kolesnikov, E. G. Ponyatovsky, and J. Tomkinson, Phys. Rev. B **58**, 2591 (1998).

[29] M. Kemali, J. E. Totolici, D. K. Ross, and I. Morrison, Phys. Rev. Lett. **84**, 1531 (2000).

[30] C. Elsässer, K. M. Ho, C. T. Chan, and M. Fähnle, J. Phys.: Condens. Matter **4**, 5207 (1992).

[31] H. Krimmel, L. Schimmele, C. Elsässer, and M. Fähnle, J. Phys.: Condens. Matter **6**, 7679 (1994).

[32] R. Caputo and A. Alavi, Mol. Phys. **10**, 1781 (2003).

[33] H. Akiba, H. Kobayashi, H. Kitagawa, M. Kofu, and O. Yamamuro, Phys. Rev. B **92**, 064202 (2015).

[34] M. J. Gillan, J. Phys. C **19**, 6169 (1986).

[35] J. W. Culvahouse and P. M. Richards, Phys. Rev. B **38**, 10020 (1988).

[36] Y. Li and G. Wahnström, Phys. Rev. B **46**, 14528 (1992).

[37] T. Skoskiewicz, Phys. Status Solidi A **11**, K123 (1972).

[38] J. E. Schirber and C. J. M. Northrup, Phys. Rev. B **10**, 3818 (1974).

[39] J. E. Schirber, J. M. Mintz, and W. Wall, Solid State Commun. **52**, 837 (1984).

[40] W. P. Halperin, Rev. Mod. Phys. **58**, 533 (1986).

[41] G. Schmid, *Clusters and Colloids* (VCH, Weinheim,1994).

[42] Y. Volokitin, J. Sinzig, L. J. de Jongh, G. Schmid, M. N. Vargaftik and I. I. Moiseevi, Nature **384**, 621 (1996).

[43] A. Pundt and R. Kirchheim, Annu. Rev. Mater. Res. **36** 555 (2006).

[44] C. Sachs, A. Pundt, R. Kirchheim, M. Winter, M. T. Reetz, and D. Fritsch, Phys. Rev. B **64**, 075408 (2001).

[45] M. Yamauchi, R. Ikeda, H. Kitagawa, and M. Takata, J. Phys. Chem. C **112**, 3294 (2008).

[46] R. Bardhan, L. O. Hedges, C. L. Pint, A. Javey, S. Whitelam, and J. J. Urban, Nature Mater. **12**, 905 (2013).

[47] R. Griessen, N. Strohfeldt, and H. Giessen, Nature Mater. **15**, 311 (2016).

[48] J. A. Eastman, L. J. Thompson, and B. J. Kestel, Phys. Rev. B **48**, 84 (1993).

[49] T. Teranishi and M. Miyake, Chem. Mater. **10**, 594 (1998).

[50] Z. Kaszkur, J. Appl. Crystallogr. **33**, 1262 (2000).

[51] M. Suleiman, N. M. Jisrawi, O. Dankert, M. T. Reetz, C. Bahtz, R. Kirchheim, and A. Pundt, J. Alloys Compd. **356-357**, 644 (2003).

[52] B. Ingham, M. F. Toney, S. C. Hendy, T. Cox, D. D. Fong, J. A. Eastman, P. H. Fuoss, K. J. Stevens, A. Lassesson, S. A. Brown, and M. P. Ryan, Phys. Rev. B **78**, 245408 (2008).

[53] C. Zlotea, F. Cuevas, V. Paul-Boncour, E. Leroy, P. Dibandjo, R. Gadiou, C. Vix-Guterl, and M. Latroche, J. Am. Chem. Soc. **132**, 7720 (2010).

[54] A. L. Bugaev, A. A. Guda, K. A. Lomachenko, V. V. Srabionyan, L. A. Bugaev, A. V. Soldatov, C. Lamberti, V. P. Dmitriev, and J. A. van Bokhoven, J. Phys. Chem. C **118**, 10416 (2014).

[55] H. Akiba, M. Kofu, H. Kobayashi, H. Kitagawa, K. Ikeda, T. Otomo, and O. Yamamuro, J. Am. Chem. Soc. in press. DOI: 10.1021/jacs.6b04970

[56] U. Stuhr, H. Wipf, T. J. Udovic, J. Weißmüller, and H. Gleiter, J. Phys.: Condens. Matter **7**, 219 (1995).

[57] U. Stuhr, H. Wipf, K. H. Andersen, and H. Hahn, Physica B **276-278**, 882 (2000).

[58] S. Janßen, H. Natter, R. Hempelmann, T. Striffier, U. Stuhr, H. Wipf, H. Hahn, and J. C. Cook, NanoStruct. Mater. **9**, 579 (1997).

[59] K. H. Rieder, M. Baumberger, and W. Stocker, Phys. Rev. Lett. **51**, 1799 (1983).

[60] R. J. Behm, V. Penka, M.-G. Cattania, K. Christmann and G. Ertl, J. Chem. Phys. **78**, 7486 (1983).

[61] H. Okuyama, W. Siga, N. Takagi, M. Nishijima, and T. Aruga, Surf. Sci. **401**, 344 (1998).

[62] M. Wilde and K. Fukutani, Phys. Rev. B **78**, 115411 (2008).

[63] M. Wilde, K. Fukutani, M. Naschitzki, and H. J. Freund, Phys. Rev. B **77**, 113412 (2008).

[64] S. Wilke, D. Hennig, and R. Löber, Phys. Rev. B **50**, 2548 (1994).

[65] R. J. Wolf, M. W. Lee, and J. R. Ray, Phys. Rev. Lett. **73**, 557 (1994).

[66] J.-F. Paul and P. Sautet, Phys. Rev. B **53**, 8015 (1996).

[67] N. Ozawa, N. B. Arboleda Jr., T. A. Roman, H. Nakanishi, W. A. Diño, and H. Kasai, J. Phys. Condens. Matter **19**, 365214 (2007).

[68] B. Lim, M. Jiang, P. H. C. Camargo, E. C. Cho, J. Tao, X. Lu, Y. Zhu, and Y. Xia, Science **324**, 1302 (2009).

[69] M. Yamauchi and H. Kitagawa, Synth. Met. **153**, 353 (2005).

[70] A. Meyer, R. M. Dimeo, P. M. Gehring, and D. A. Neumann, Rev. Sci. Instrum. **74**, 2759-2777 (2003).

[71] J.R.D. Copley and J.C. Cook, Chem. Phys. **292**, 477 (2003).

[72] N. Rosov, S. Rathgeber, and M. Monkenbusch, ACS Symp. Ser. **739**, 103 (2000).

[73] M. Monkenbusch, R. Schätzler, and D. Richter, Nucl. Inst. Meth. Phys. Res. A **399**, 301 (1997).

[74] T. Unruh, J. Neuhaus and W. Petry, Nucl. Inst. Meth. Phys. Res. A **580**, 1414 (2007).

[75] W. Lohstroh and Z. Evenson, J. Large-scale Res. Facil. **1**, A15 (2015).

[76] R. T. Azuah, L. R. Kneller, Y. Qiu, P. L. W. Tregenna-Piggott, C. M. Brown, J. R. D. Copley, and R. M. Dimeo, J. Res. Natl. Inst. Stan. Technol. **114**, 341 (2009).

[77] O. Arnold *et al.*, Nucl. Instr. Meth. Phys. Res. A **764**, 156 (2014).

[78] C. T. Chudley and R. J. Elliott, Proc. Phys. Soc. **77** 353 (1961).

[79] D. A. Cornell and E. F. W. Seymour, J. Less-Common Met. **39**, 43 (1975).

[80] I Svare, Physica **141B**, 271 (1986).

[81] V. Lottner, J. W. Haus, A. Heim, and K. W. Kehr, J. Phys. Chem. Solids **40**, 557 (1979).

[82] L. Schimmele and A. Klamt, J. Phys.: Condens. Matter **4**, 3405 (1992).

[83] H. Grönbeck and V. P. Zhdanov, Phys. Rev. B **84**, 052301 (2011).

[84] F. Calvo and D. Costa, J. Chem. Theory Comput. **6**, 2 (2010).